

Short Communication

## Aggregation of MAO Coatings and Crack Formation in the Microgrooves on an Aluminum Surface

Manxi Sun <sup>1</sup>, Hongjian Huang <sup>1, \*</sup>, Xiaowei Wei <sup>2</sup>, Jianhui Qiu <sup>1</sup>

<sup>1</sup> Department of Machine Intelligence and Systems Engineering, Faculty of Systems Engineering, Akita Prefectural University, Akita 015-0055, Japan

<sup>2</sup> School of Materials Science and Engineering, Xihua University, Chengdu 610039, PR China

\*E-mail: [hongjianhuang1021@yeah.net](mailto:hongjianhuang1021@yeah.net)

Received: 4 September 2019 / Accepted: 1 November 2019 / Published: 30 November 2019

---

Surface microgroove pretreatment has been proven to be an effective method to increase the formation efficiency and performance of microarc oxidation (MAO) coatings. Here, the effect of the microgroove dimensions on an MAO coating was investigated systematically. The results indicate that as the opening angles of the microgrooves decrease, the coating aggregation increases and the defects become very obvious. Conversely, microgrooves that are too large lose their effect on the coating. Moreover, the MAO coatings in the central region of the microgrooves are mainly composed of a nodular structure contrasting to the volcanic structure of the planar regions.

---

**Keywords:** Micro-arc oxidation; Microgrooves; Microstructure; Defects.

### 1. INTRODUCTION

Microarc oxidation (MAO) or plasma electrolytic oxidation (PEO) [1, 2] is a relatively new surface treatment technology that is used to produce ceramic coatings on lightweight alloys, e.g., aluminum, magnesium, titanium, and zirconium [3] by the so-called plasma discharge process [4]. MAO coatings possess excellent qualities, e.g., wear resistance [5], corrosion resistance [1,2], and thermal shock resistance [6]. However, the growth process of MAO coatings is violent, accompanied by complex plasma electrochemical reactions and hard to control. Most of the applied electrical energy is wasted on heating the electrolyte, resulting in a low coating growth rate and limited applications. Many factors affecting the growth of MAO coatings, e.g., the electrical parameters [7, 8], electrolyte composition [9, 10], powder additives [1, 2], and substrate composition [11], and these have been extensively discussed in previous studies, but the improvements are still limited. In contrast, a mechanical surface pretreatment before the MAO process, which is a simple, effective and environmentally friendly approach, has

attracted increasing attention, e.g., by shot-peening, mechanical attrition and honeycomb pretreatments [12-14]. Recently, microgrooving pretreatments have been applied to aluminum alloys to increase the growth rate and wear resistance of coatings [15]. Wang et al. [16] noted that the sharp-angled effect resulted in the uneven distribution of the electric field around the microgrooves so that obvious discharge channels would form in the MAO coating at the center of the microgrooves. However, in our subsequent experiments, it was found that the MAO coating in the microgroove tended to form defects while growing rapidly. Therefore, further studies are still needed to investigate the MAO coating growth behavior on aluminum with microgrooves.

In this letter, MAO coatings were fabricated in a silicate solution. The aggregation and crack initiation behaviors of the MAO coatings in the microgrooves with different dimensions were investigated by using scanning electron microscopy (SEM).

## 2. EXPERIMENTAL PROCEDURES

Commercially pure aluminum was cut into rectangular pieces (25 mm×25 mm×5 mm), and then one trapezoidal microgroove was machined onto the surface of the samples, as shown in Fig. 1. A siliceous solution containing 15 g/L Na<sub>2</sub>SiO<sub>3</sub>·9H<sub>2</sub>O and 2 g/L KOH in deionized water was used as the electrolyte (pH=11~12, temperature ≤ 30°C). The sample and a stainless steel plate served as the anode and cathode, respectively. To investigate the growth behavior of the MAO coating at the bottom of the microgrooves, the MAO processes were carried out for different times (30, 90, 120 and 150 min). Both the positive and negative current densities were maintained at 20 A/dm<sup>2</sup>, the frequency was 200 Hz and the duty cycle was 50.0%. After MAO treatment, the samples were washed with deionized water and then dried at room temperature for characterization.

Scanning electron microscopy (SEM, FEI Quanta FEG 250) was used to observe the microstructures of the coatings. Prior to examination, the samples were cut, mounted in resin, and polished through successive grades of SiC abrasive papers.

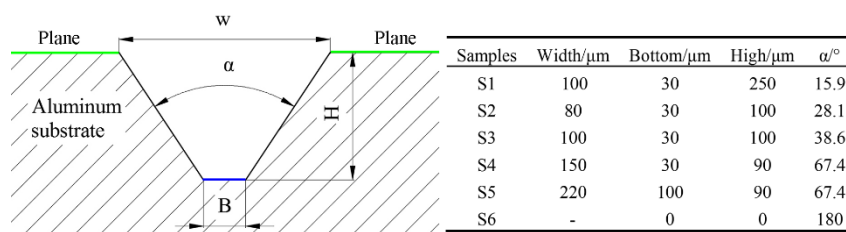
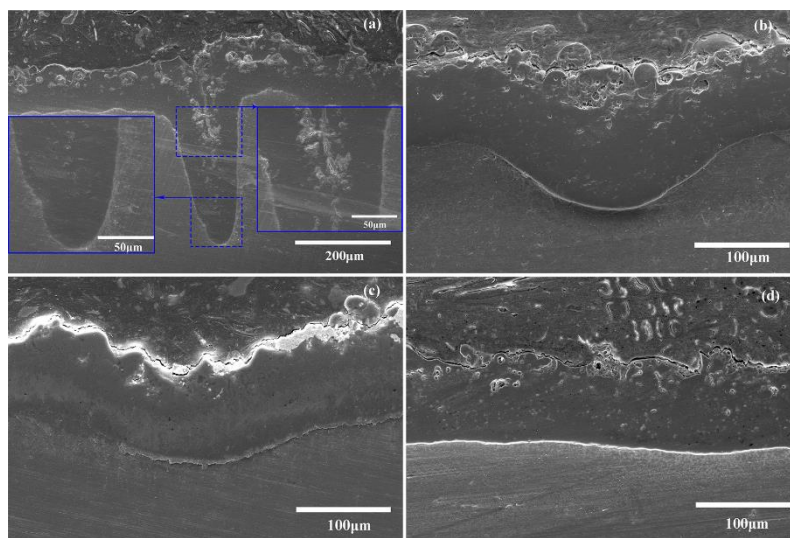


**Figure 1.** The machining dimensions of the microgrooves.

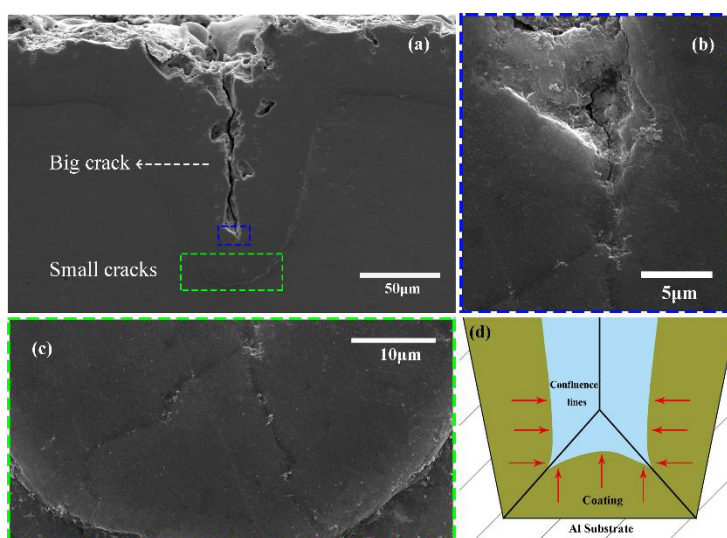
## 3. RESULTS AND DISCUSSION

Fig. 2 shows the cross-sectional morphologies of the MAO coatings processed on the aluminum substrates. A tapered coating was produced on sample S1, a zigzag coating was generated on sample S4, a wavy coating was formed on sample S5, and a linear coating was designed on sample S6 for

comparison. Notably, a long and narrow crack can be clearly observed on sample S1 (Fig. 2a). The crack extends to the interior of the coating from the surface and is surrounded by many micropores. The micropores should be considered as the legacy of gas molecules in the cooled and solidified coating [3]. In contrast, an appropriate value of  $\alpha$  is helpful for forming MAO coatings with decreased porosity (Fig. 2b,  $\alpha=67.4^\circ$ ). However, when the value of B is larger than 100  $\mu\text{m}$  (S5, Fig. 2c), the MAO coatings cannot connect at the bottom, resulting in a wavy MAO coating. In general, the MAO coating at the bottom of microgrooves can largely maintain the original structure of the microgrooves.



**Figure 2** MAO coatings prepared on different substrate samples for 150 min: (a) S1, (b) S4, (c) S5, and (d) S6.



**Figure 3.** The cross-sectional morphologies of the coating processed on S2 for 90 min (a, b and c) and the proposed sketches for crack growth (d).

Fig. 3 shows the cross-sectional morphologies of the MAO coating processed on sample S2 for 90 min. Clearly, the coating grows face to face in the microgroove, and two small cracks appear earlier than a large crack (Fig. 3a). The cracks undoubtedly are the boundary of different coating surfaces, i.e., two inclined surfaces and one bottom surface (Fig. 3d). Fig. 3b presents the typical process in which the molten coating material ejected by the microdischarge from the left inclined coating surface hits the right inclined coating surface. After the microdischarge is quenched, the coating material rapidly freezes, and the crack grows. Thus, the cracks can be regarded as a kind of weld line.

Fig. 4 shows the MAO coating processed on sample S2 for 120 min. The microgroove is filled with the coating materials, leaving one crack (~80 nm long, as shown in Fig. 4a and c). On the surface of the planar area (Fig. 4b), two representative structures of the MAO coating can be observed, i.e., accumulated particles with a nodular structure and a resolidified pool with a central hole [15]. In contrast, additional nodular particles can be observed around the microgroove (Fig. 4a). The absence of resolidified pools around the microgroove indicates that it is difficult for the electric breakdown from the bottom of the microgroove to reach the coating surface along the crack. Therefore, the dielectric breakdown, which is perpendicular to the large weld line, might become the only way to maintain the evolution of the MAO coating around the weld line (Fig. 4d).

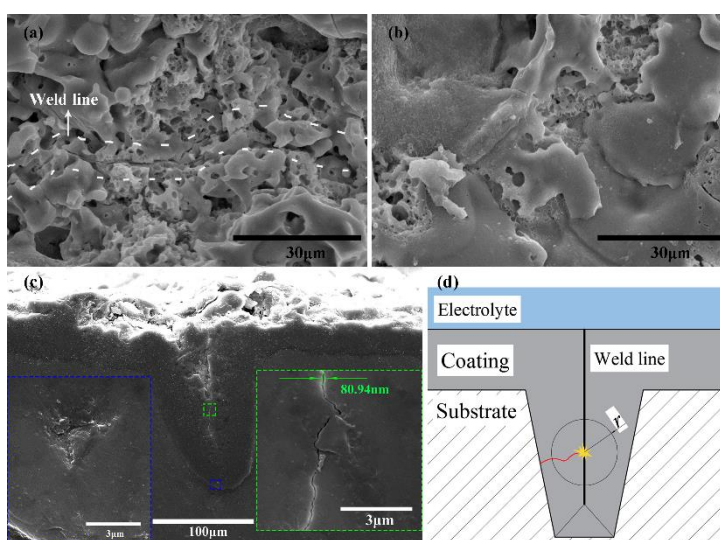


**Figure 4.** The morphologies of the coating processed on sample S2 for 120 min: (a) and (b) the surface morphologies of the microgroove and plane area, respectively; (c) the cross-sectional morphology; and (d) for a schematic of the proposed plasma discharge process.

Fig. 5 shows the growth process of the MAO coating on sample S3. The strong current sharp-angled effect is reflected by the uneven coating thickness during the early MAO process (Fig. 5a). The crack location appears at the edge of the microgroove instead of the bottom corner, which is contrary to the literature [16]. With increasing MAO time, the thickened coatings from the three directions meet at the bottom of the microgroove (Fig. 5c). In fact, the microgroove in sample S3 was closed at a slower speed than that of samples S2 and S1; thus, the nodular oxide (Fig. 5e) ejected from the discharge channels have enough time to be soldered together perfectly by the plasma discharges. The appropriate

value of  $\alpha$  (sample S3,  $38.6^\circ$ ) provides a good way for gases to escape and suppresses the generation of pores.

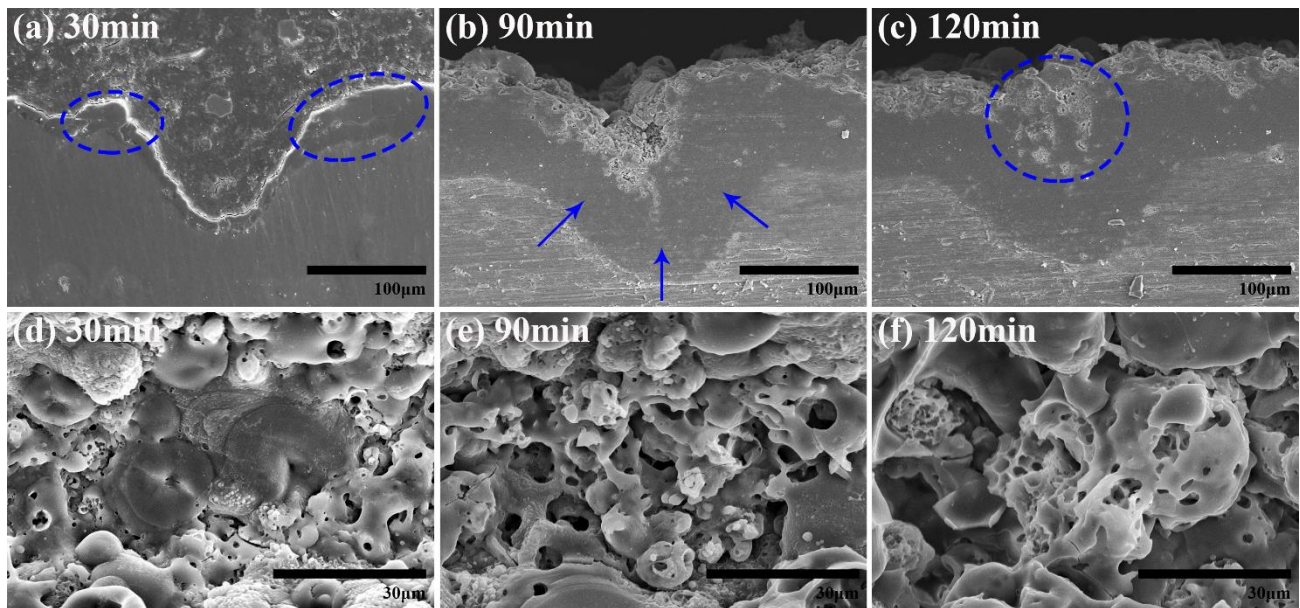


**Figure 5.** The morphologies of coatings processed on S3: (a, b and c) cross sections and (d, e and f) the surface.

#### 4. CONCLUSIONS

The structure of MAO coatings depends on the dimensions of the microgrooves, and the coating defects increase with a decrease in the opening angle. The microgrooves with an appropriate size have an aggregation effect on ejected products, which accelerates the coating growth. To retain the effect of microgrooves without weld lines, an appropriate value of  $\alpha$  should be maintained at approximately  $38.6\sim 67.4^\circ$ .

#### ACKNOWLEDGEMENTS

Dr. Sun and Dr. Huang would like to thank the financial support from the program of China Scholarships Council (No. 201708510090 and 201708510091). This work was supported by the Chunhui project under Grant (Z2011074).

#### References

1. P. Wang, T. Wu, Y. Xiao, J. Pu, X. Guo, *Mater. Lett.*, 182 (2016) 27.
2. P. Wang, T. Wu, H. Peng, X. Guo, *Mater. Lett.*, 170 (2016) 171.
3. Y. Cheng, T. Wang, S. Li, Y. Cheng, J. Cao, H. Xie, *Electrochim. Acta*, 225 (2017) 47.
4. A. L. Yerokhin, X. Nie, A. Leyland, A. Matthews, S. J. Doweyc, *Surf. Coat. Technol.*, 122 (1999) 73.
5. J. Wang, S. Huang, H. Huang, M. He, P. Wangyang, L. Gu, *J. Alloys Compd.*, 777 (2019) 94.

6. J.A. Curran, H. Kalkancı, Yu. Magurova, T.W. Clyne, *Surf. Coat. Technol.*, 201 (2007) 8683.
7. J. Wang, M. Du, F. Han, J. Yang, *Appl. Surf. Sci.*, 292 (2014) 658.
8. J. Martin, A. Melhem, I. Shchedrina, T. Duchanoy, A. Nominé, G. Henrion, T. Czerwiec, T. Belmonte, *Surf. Coat. Technol.*, 221 (2013) 70.
9. A. Polat, M. Makaraci, M. Usta, *J. Alloys Compd.*, 504 (2010) 519.
10. H. Luo, Q. Cai, B. Wei, B. Yu, D. Li, J. He, Z. Liu, *J. Alloys Compd.*, 464 (2008) 537.
11. A. E. Gulec, Y. Gencer, M. Tarakci, *Surf. Coat. Technol.*, 269 (2015) 100.
12. D.T. Asquith, A.L. Yerokhin, J.R. Yates, A. Matthews, *Thin Solid Films*, 516 (2007) 417.
13. L. Wen, Y. Wang, Y. Zhou, L. Guo, J. Ouyang, *Corros. Sci.*, 53 (2011) 473.
14. X. Wei, H. Huang, M. Sun, W. Liu, J. Qiu, *Surf. Coat. Technol.*, 363 (2019) 265.
15. H. Huang, X. Wei, J. Yang, J. Wang, *Appl. Surf. Sci.*, 389 (2016) 1175.
16. J. Wang, S. Huang, M. He, P. Wangyang, Y. Lu, H. Huang, L. Xu, *Ceram. Int.*, 44 (2018) 7656.

© 2020 The Authors. Published by ESG ([www.electrochemsci.org](http://www.electrochemsci.org)). This article is an open access article distributed under the terms and conditions of the Creative Commons Attribution license (<http://creativecommons.org/licenses/by/4.0/>).